Diabetology & Metabolic Syndrome

RESEARCH

Open Access

Histopathological insights and therapeutic prospects of MCC950 in diabetes-associated autonomic-related structural alterations in a type 1 diabetes Wistar rat model

Shamala Devi Subramaniam[1], Juita Chupri[2], Zamzarina Ahmad Bajari[2], Xin Yi[3] and Razif Abas[4*]

Abstract

Diabetes-Associated Autonomic-Related Structural Alterations (DAAS) is a severe complication of type 1 diabetes mellitus (T1DM) characterized by autonomic nerve fiber dysfunction in the heart and blood vessels. This study aimed to elucidate the histopathological mechanisms underlying DAAS and evaluate the therapeutic potential of MCC950, an NLRP3 inflammasome inhibitor, in a Wistar rat model. Male Wistar rats were divided into control and T1DM groups, with diabetes induced by streptozotocin (STZ) injection. Following confirmation of DAAS through elevated serum noradrenaline levels, diabetic rats were subdivided into positive control (insulin-treated), treatment (MCC950), and untreated groups. The stellate ganglia, thoracic aorta, and left ventricle were dissected for histological examination using Haematoxylin and Eosin (H&E) and Masson Trichrome staining. STZ-induced hyperglycemia was evident by Week 1 and sustained throughout the study. Serum noradrenaline levels significantly increased by Week 14 in diabetic rats, indicating DAAS onset. Histological analysis revealed atrophy in stellate ganglia, endothelial damage in the thoracic aorta, and myocardial fibrosis in untreated diabetic rats. MCC950 treatment preserved ganglionic structure, mitigated vascular damage, and reduced myocardial fibrosis, demonstrating its potential in attenuating DAAS progression. These findings highlight MCC950 as a promising therapeutic agent for DAAS by targeting inflammation and preserving autonomic and cardiovascular function. Further investigations are warranted to validate MCC950's efficacy in human trials, with the potential to improve clinical outcomes for T1DM patients at risk of DAAS.

Keywords Diabetes-associated autonomic-related structural alterations (DAAS), Type 1 diabetes mellitus (T1DM), MCC950, NLRP3 inflammasome, Histopathology

*Correspondence:
Razif Abas
razifabas@upm.edu.my
[1]Department of Medical Microbiology, Faculty of Medicine and Health Sciences, Universiti Putra Malaysia, Serdang 43400, Selangor, Malaysia
[2]Department of Pathology, Faculty of Medicine and Health Sciences, Universiti Putra Malaysia, Serdang 43400, Selangor, Malaysia
[3]Department 1 of Cardiovasology, North China University of Science and Technology Affiliated Hospital, Tangshan City 063000, Hebei Province, China
[4]Department of Human Anatomy, Faculty of Medicine and Health Sciences, Universiti Putra Malaysia, Serdang 43400, Selangor, Malaysia

Introduction

Diabetes-associated autonomic-related structural alterations (DAAS) represents a significant complication of type 1 diabetes mellitus (T1DM) with far-reaching implications for cardiovascular health [1]. In T1DM, the autonomic nervous system, responsible for regulating involuntary bodily functions including heart rate and blood pressure, becomes dysregulated. DAAS manifests as a progressive dysfunction of autonomic nerve fibers innervating the heart and blood vessels, leading to abnormalities in heart rate variability, impaired baroreflex sensitivity, and altered vascular responses [2]. These disruptions contribute to an increased risk of arrhythmias, myocardial ischemia, and sudden cardiac death, underscoring the clinical importance of understanding and managing DAAS in T1DM patients [3].

Extensive research has been conducted to unravel the intricate histopathology of DAAS in T1DM. Studies have implicated multiple mechanisms, including inflammation, endothelial dysfunction, and neurohormonal imbalance, in the development and progression of DAAS [4]. Chronic hyperglycaemia promotes the formation of advanced glycation end-products (AGEs) and activates inflammatory pathways, leading to neuronal damage and dysfunction within the autonomic nervous system. Furthermore, dysregulation of neurohormonal signalling, such as increased sympathetic activity and blunted parasympathetic function, exacerbates cardiac dysautonomia and perpetuates the vicious cycle of DAAS progression [5]. Chronic inflammation plays a central role in the pathogenesis of DAAS [6]. Hyperglycaemia and advanced glycation end-products activate inflammatory pathways, resulting in the release of proinflammatory cytokines and oxidative stress, which contribute to neuronal damage within the autonomic nervous system [7]. These inflammatory processes further exacerbate autonomic dysfunction by promoting myocardial fibrosis, vascular remodeling, and myocyte loss [8, 9], ultimately impairing cardiac autonomic regulation and leading to functional deficits such as reduced heart rate variability and impaired baroreflex sensitivity [10]. Understanding the role of inflammation in DAAS provides a rationale for exploring anti-inflammatory therapeutic strategies to prevent or attenuate disease progression.

Diabetic cardiac autonomic neuropathy is characterized by a range of histopathological alterations within the heart and its autonomic innervation [6]. These changes include degeneration and loss of autonomic nerve fibers [11], neuronal atrophy in the stellate ganglia [12], fibrosis of the myocardium and remodeling of the vascular walls [7]. In addition, inflammation and oxidative stress contribute to structural damage, including myocyte loss, disorganized cardiac fibers, and increased extracellular matrix deposition [13]. Collectively, these histological alterations underlie the functional impairments observed in DAAS, such as reduced heart rate variability, impaired baroreflex sensitivity, and altered vascular responses.

Despite advances in understanding DAAS histopathology, therapeutic options for preventing or reversing its progression remain limited. Current approaches primarily focus on glycaemic control, and lifestyle modifications to mitigate cardiovascular risk factors associated with T1DM [14]. Current clinical management of DAAS focuses primarily on maintaining glycaemic control and mitigating cardiovascular risk factors, such as hypertension and dyslipidaemia, through pharmacological therapy and lifestyle interventions [15]. Some medications, including angiotensin-converting enzyme inhibitors, angiotensin receptor blockers, and selected antidiabetic agents, have been employed to improve autonomic function [16]. However, these strategies have shown limited success in preventing or reversing the progression of DAAS, as they mainly target metabolic or hemodynamic aspects rather than the underlying neurodegenerative and inflammatory processes. This highlights a critical need for novel therapeutic approaches that directly address the pathophysiology driving cardiac autonomic dysfunction in diabetes.

One promising avenue of research involves the investigation of MCC950, a potent inhibitor of the NLRP3 inflammasome, in the treatment of DAAS. The NLRP3 inflammasome is a key mediator of inflammation and oxidative stress implicated in the pathogenesis of diabetes and its complications [17, 18]. Preclinical studies have shown that MCC950 administration attenuates inflammatory responses, preserves autonomic function, and improves cardiovascular outcomes in diabetic animal models [19]. By targeting the inflammatory cascade underlying DAAS histopathology, MCC950 holds promise as a novel therapeutic agent for preventing or delaying the onset of DAAS and its associated complications in T1DM patients.

Moreover, investigations into the structural alterations within key anatomical structures such as the stellate ganglia, thoracic aorta, and left ventricle have provided valuable insights into the pathological changes associated with DAAS [20]. Diabetes type I induction in Wistar rats, commonly achieved through Streptozotocin (STZ) injections, mimics the hyperglycaemic state observed in T1DM patients and facilitates the study of DAAS progression [21]. Blood pressure and heart rate monitoring techniques allow for the assessment of autonomic dysfunction and cardiovascular abnormalities associated with DAAS [2]. Noradrenaline measurement serves as a marker of sympathetic activity and provides insight into the dysregulation of neurohormonal signalling in DAAS [14]. Dissection and histological examination of the stellate ganglia, thoracic aorta, and left ventricle reveal

structural alterations indicative of neuronal damage, vascular remodelling, and myocardial fibrosis characteristic of DAAS [22]. Haematoxylin and Eosin staining elucidate morphological alterations [23], while Masson Trichrome staining highlights collagen deposition and fibrotic changes within the myocardium and blood vessel walls, providing further insights into the structural remodelling underlying DAAS progression [24]. These histological techniques offer valuable tools for characterizing the histopathological changes associated with DAAS and evaluating the efficacy of novel therapeutic interventions, such as MCC950 [20].

The objectives of this study are twofold: first, to elucidate the histopathological mechanisms underlying DAAS in T1DM, focusing on the role of the autonomic nervous system and its interaction with diabetic metabolic derangements; second, to evaluate the therapeutic potential of MCC950, an anti-inflammasome agent, in attenuating DAAS progression in a preclinical model. By addressing these objectives, we aim to contribute to a more comprehensive understanding of DAAS in T1DM and provide insights into novel therapeutic avenues for its management. Through rigorous experimentation and analysis, we seek to bridge the current gaps in knowledge and pave the way for improved clinical outcomes for T1DM patients at risk of DAAS-related complications.

Methods and materials

Animals

Forty Male Wistar rats, 6weeks old and weighing between 180 and 200 g were procured from the Comparative Medicine and Technology Unit (COMeT). Ethical approval for animal handling was obtained from the Institutional Animal Care and Use Committee (IACUC). The rats were housed in the Animal Behaviour Laboratory within the Human Anatomy Department, in sanitized cages under controlled environmental conditions, maintaining a 12-hour light/dark cycle, regulated temperature (25 ℃), and humidity (50%) levels. A period of two weeks was allotted for the rats to acclimatize to their new environment before the commencement of the experiments. Throughout the adaptation phase, the rats were accommodated in pairs in wooden cages and provided ad libitum access to standard rat pellets [25]. All experimental procedures adhered to the Animal Research Reporting of In Vivo Experiments (ARRIVE) guidelines.

T1DM induction

Following the adaptation period, the rats were randomly assigned to two groups: a Control group (n = 10) and an experimental group (n = 30). The experimental group received intraperitoneal injections of a high dose of STZ at 50 mg/kg [21], with the aim of establishing T1DM model. Subsequently, while maintaining their regular diet and housing conditions, all rats remained untreated until the onset of DAAS was established.

Before the morning fasting blood glucose (FBG) assessment using an Accu-check Guide Meter glucometer, rats underwent fasting starting from 20:00 the preceding evening. FBG levels were monitored every weeks, the experiment started from Week 0 (baseline), and subsequent time points were recorded weekly as Week 1, Week 2, up to Week 18. Blood samples were obtained from the tail of each rat following sterilization with an alcohol swab. A small section (approximately 3 mm) of the tail tip was excised, and the blood glucose test paper was inserted into the glucometer for analysis [26]. Each FBG measurement was performed in triplicate for each rat to ensure accuracy.

The onset of T1DM in the experimental group was considered triggered when FBG levels showed a statistically significant increase compared to the control group and exceeded 250 mg/dL (13.9 mmol/L). This threshold was based on established criteria for T1DM induction in rodent models [27].

Noradrenaline (NA) measurement

Following appropriate anaesthesia induction with the ketamine/xylazine recipe delivering 80 mg/kg ketamine and 8 mg/kg xylazine, these formulations were prepared in sterile vials using specified dilutions of stock drugs and 0.9% saline diluent. They were then administered intraperitoneally at a dosage of 0.1 mL/100 g [28]. Afterward, 0.5 ml of normal saline was administered intraperitoneally to prevent cannibalism. Whole blood samples for NA measurement were collected using disposable test tubes in accordance with the manufacturer's instructions (Elabscience Biotechnology, China) at Week 10 and Week 14. The rats exhibited a reversal of sedative effects within 2 h simultaneously. The competitive ELISA principle was employed by the ELISA kit utilized. The provided ELISA plate had been pre-coated with Noradrenaline/Norepinephrine (NA/NE). During the reaction, NA in the samples or standard competed with a fixed amount on the solid-phase supporter for sites on the Biotinylated Detection Ab Specific to NA. Subsequently, excess conjugate and unbound samples were thoroughly washed from the plate, and Avidin conjugated to Horseradish Peroxidase (HRP) was introduced into the microplate well and allowed to incubate. Following this, the TMB substrate solution was added to each well. The enzyme-substrate reaction was halted by the addition of a stop solution, and the resulting colour change was spectrophotometrically measured at a wavelength of 450 nm. The concentration of NA in the samples was determined by comparing the optical density (OD) of the samples to the standard curve (Al-Assi et al., 2018). Each sample was measured in duplicate to ensure reliability.

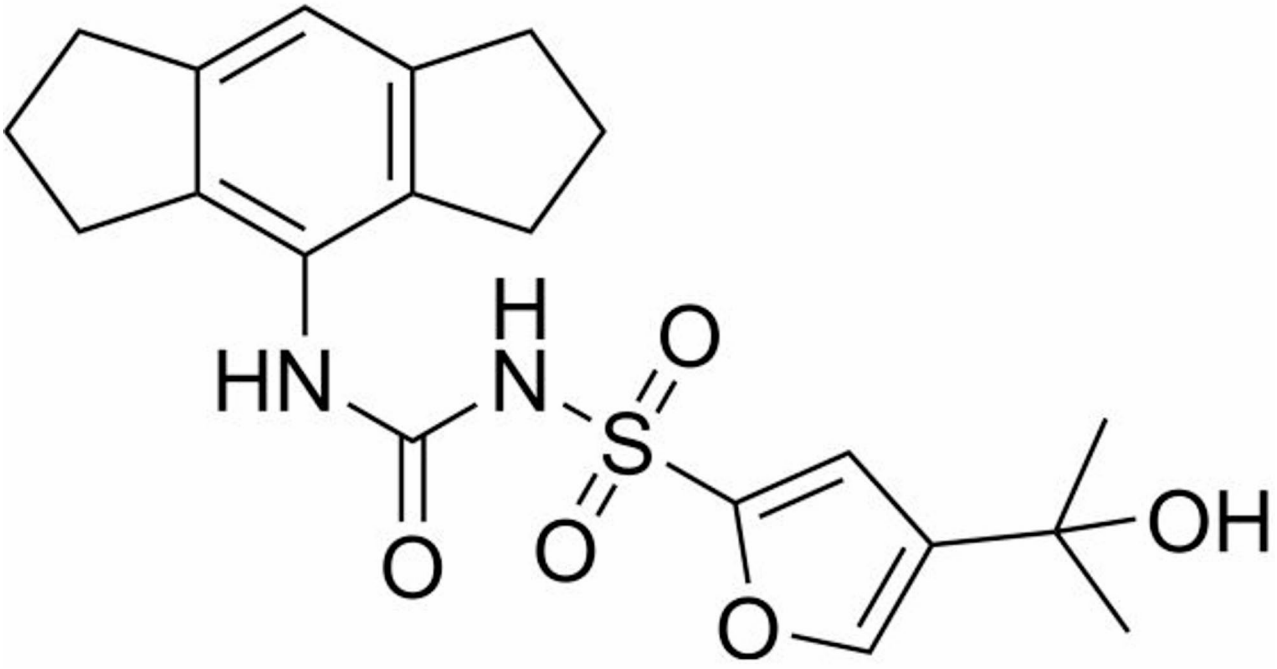

Fig. 1 Chemical structure of MCC950 sodium (C20H23N2NaO5S).

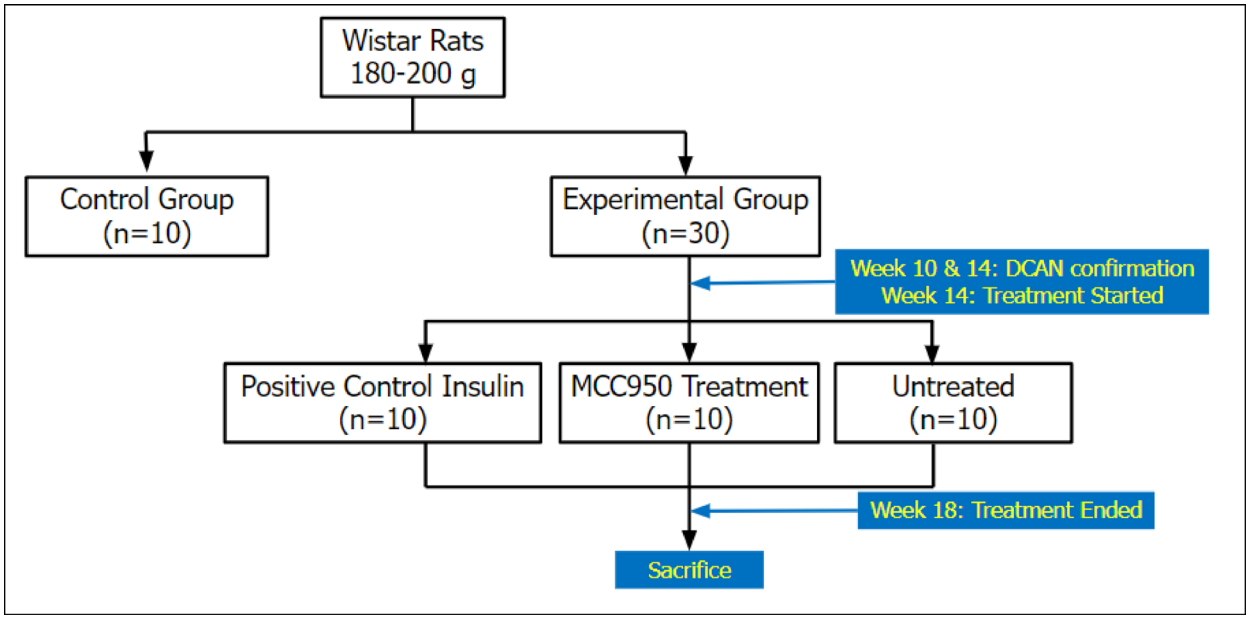

Fig. 2 The schematic diagram illustrated four groups of rats: a non-diabetic control group, an experimental diabetic positive control group treated with insulin, treated with MCC950, and an untreated diabetic group, with $n = 10$ in each group

MCC950 treatment

After the establishment of DAAS was confirmed by the evidence of increased NA levels in the experimental group [23], they were randomly subdivided into three subgroups: positive control, treatment, and untreated groups. The initial control group remained as the negative control group. The positive control group received insulin at 5.0 U/kg/day (Zhu et al., 2018), the treatment group was administered IP MCC950 at 3 mg/kg/day [29, 30], and the untreated group received normal saline 5 mg/kg. MCC950 (sodium salt) was purchased from MedChemExpress (Monmouth Junction, NJ, USA; Cat. No. HY-12815), and its chemical structure is shown in Fig. 1. All groups were administered intraperitoneally for 4 weeks (Fig. 2).

Stellate ganglia, thoracic aorta and left ventricle dissection

The stellate ganglia, thoracic aorta, and left ventricle dissection procedures were meticulously conducted with the aid of Motic's stereoscopic microscope to elucidate the structural and histological changes associated with DAAS in Wistar rats [31]. Each tissue type was sampled from 10 rats per group for histological analysis. Following sacrifice, induced by administering a dosage similar to that of the sedative group but without normal saline, the rats were positioned supine, and a midline incision was made along the ventral abdomen to expose the thoracic cavity. Careful attention was given to minimize tissue trauma and maintain physiological integrity throughout the dissection process.

The stellate ganglia were located bilaterally adjacent to the base of the heart, in close proximity to the sympathetic trunk [32]. Using fine dissection scissors and forceps, the stellate ganglia were carefully dissected free from surrounding connective tissue and excised (Fig. 3). Special care was taken to preserve the anatomical integrity of the ganglia to facilitate subsequent histological analysis [33].

Haematoxylin and eosin staining

The stellate ganglia and thoracic aorta were collected and preserved in a 10% formalin saline solution for 24 h before being prepared for staining. The fixed tissues were then transferred to the hardening process using paraffin blocks and cut into sections with a thickness of 5 µm. For histological analysis, the sections were mounted on standard glass slides and stained with Haematoxylin and Eosin [34]. This process was conducted using a Nikon microscope at a magnification of 400X. For the semi-quantitative measurement of the stellate ganglia, the average measurement of the 4-shrinkage gap area of each nerve cell was measured using DinoCapture 2.0 (Dino-Lite, China). A minimum of 6 sections per tissue per animal were analyzed to ensure representative sampling. For each section, 10 non-overlapping fields were randomly selected, and within each field, 10 cells were randomly chosen for measurement [35].

Masson trichrome staining

Following similar preservation and sectioning procedures, paraffin blocks containing the left ventricle were prepared for the analysis of collagen content in the

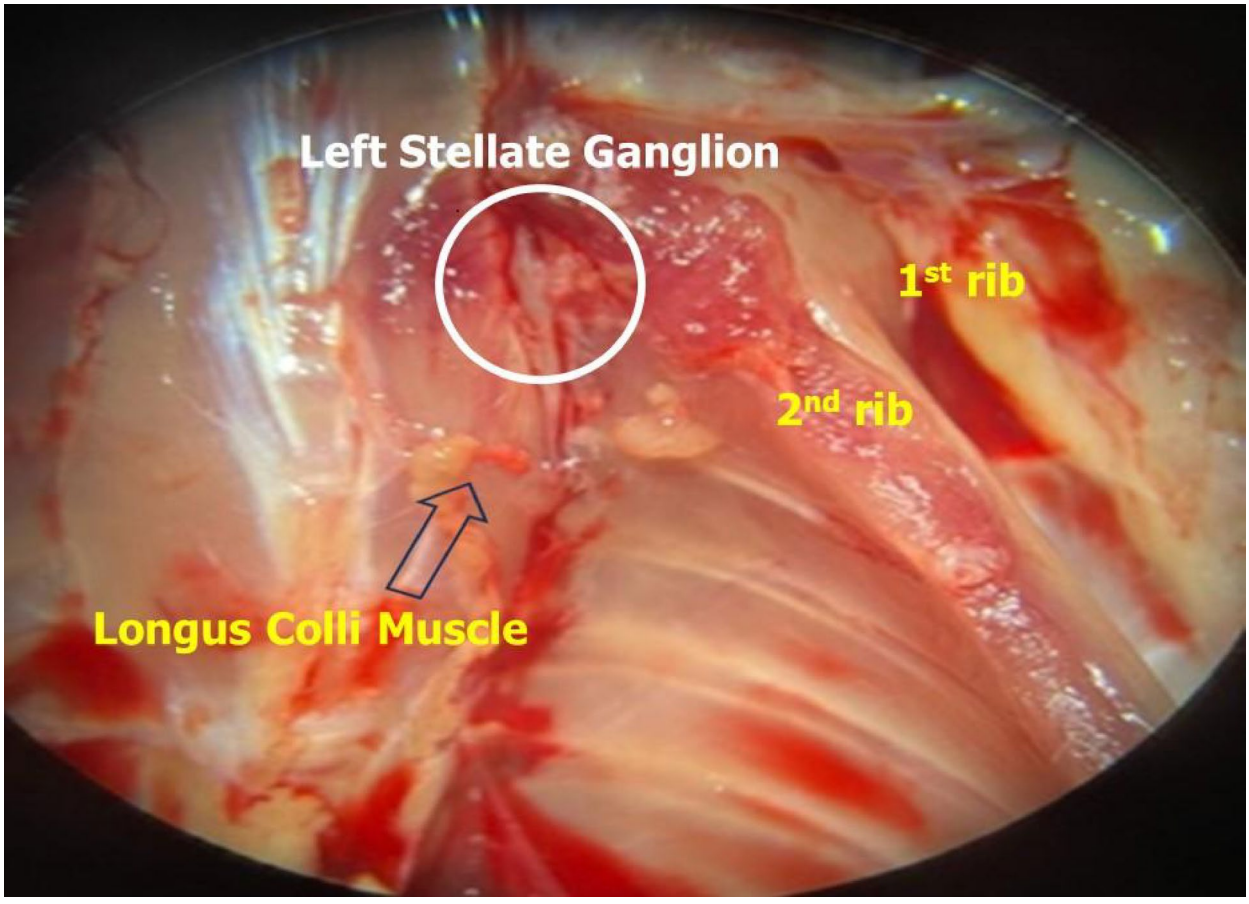

Fig. 3 After sacrifice, the gross features of the dissected left stellate ganglion of the Wistar rats were examined. Careful dissection under microscopy aided in identifying nearby landmarks such as the longus colli muscle, 1st and 2nd rib

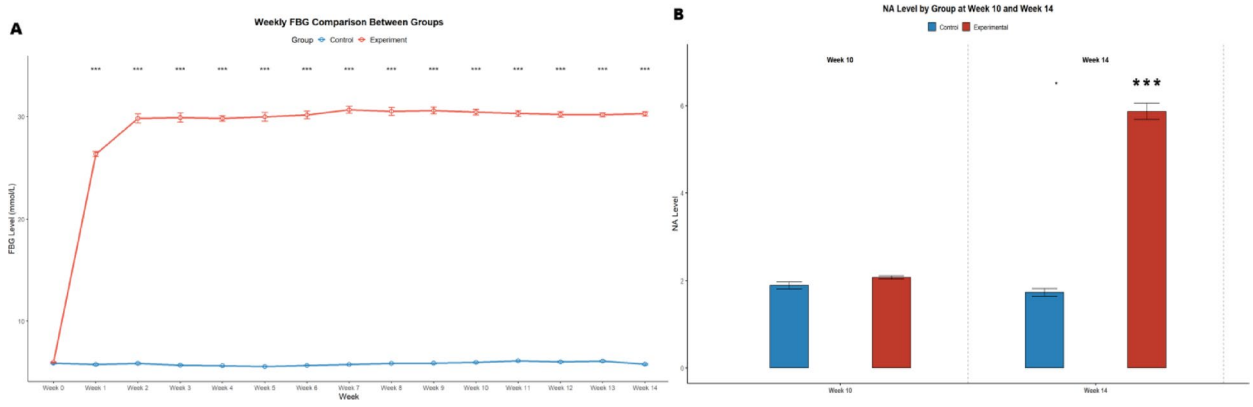

Fig. 4 **A**: FBG trends from Week 1 to Week 15; **B**: Comparison of NA levels between groups at Week 10 and Week 14. (***: $P < 0.001$)

endocardium, perivascular area, and myocardium of the fibrosed left ventricle. Masson's trichrome stain was used on tissue slices of the rat heart for this purpose. Following similar preservation and sectioning procedures, paraffin blocks containing the left ventricle were prepared for the analysis of collagen content in the endocardium, perivascular area, and myocardium of the fibrosed left ventricle. Masson's trichrome stain was used on tissue slices of the rat heart for this purpose. Furthermore, semi-quantitative analysis of cardiomyocyte size was performed by measuring the width and length of each cell in cross-section, and the mean of these two values was calculated using DinoCapture 2.0 (Dino-Lite, China). A minimum of 6 sections per tissue per animal were analyzed to ensure representative sampling. For each section, 10 non-overlapping fields were randomly selected, and within each field, 10 cells were randomly chosen for measurement [36].

Statistical analysis

Statistical analysis was conducted using R (4.5.0) and PRISM version 19, Statistical analysis were conducted using independent t-tests for comparisons between two groups, one-way ANOVA followed by Tukey HSD test for multiple group comparisons, paired t-tests for comparisons between two different time points within the same group. All analyses were considered statistically significant at $P < 0.05$.

Results

Establishment of T1DM and DAAS models

T1DM was induced by STZ. 1 week after injection, FBG in the Experimental Group increased significantly to approximately 26 mmol/L compared to the Control group ($P < 0.001$), indicating successful T1DM induction. From Week 1 to Week 2, FBG continued to rise, and thereafter remained stable at around 30 mmol/L until Week 14, suggesting persistent hyperglycemia in the Experimental group. (Fig. 4A). NA was first assessed at Week 10, showing no significant difference between 2 groups. However, at Week 14, NA in the Experimental Group was markedly higher than in the Control Group ($P < 0.001$), indicating that the DAAS model was successfully established at this time point (Table 1; Fig. 4B).

Table 1 Comparison of NA levels between groups at Week 10 and Week 14

Weeks	Group	NA (uL)	t	*P*
Week 10	Control ($n = 10$)	1.89 ± 0.25	-2.078	0.059
	Experiment ($n = 30$)	2.07 ± 0.19		
Week 14	Control ($n = 10$)	1.73 ± 0.28	−19.968	< 0.001
	Experiment ($n = 30$)	5.87 ± 1.02		

The effects of MCC950 on FBG

Following the establishment of the DAAS model, MCC950 treatment was administered for 4 weeks. A continuous decline in FBG levels was observed in both the Treatment Group (MCC950 intervention) and the Positive Control Group (insulin intervention). However, during the first three weeks of treatment (Week 15, Week 16, and Week 17), no significant differences in FBG levels were observed between these groups and the Untreated Group. By Week 18, both Treatment and Positive Control Groups exhibited significantly lower FBG levels compared to the Untreated Group ($P < 0.01$), suggesting that 4 weeks of MCC950 or insulin administration effectively reduced FBG. Notably, at all assessed time points, there were no statistically significant differences in FBG levels between the Treatment Group and the Positive Group, indicating comparable FBG-lowering efficacy between the two treatments (Table 2; Fig. 5).

The effects of MCC950 on stellate ganglia

Histologically, the stellate ganglia showed normal architecture in the negative control group, while the untreated group exhibited atrophy characterized by a decrease in ganglionic size and cell density, reflecting the gradual loss of neurons and structural alterations within the

Table 2 Comparison of FBG levels between 4 groups from Week 15 to Week 18

Weeks	Group	FBG (mmol/L)	F	*P*
Week 15	Negative Control ($n=10$)	5.70 ± 0.27	1.617	0.217
	Positive Control ($n=10$)	30.40 ± 0.87		
	Treatment ($n=10$)	28.70 ± 4.12		
	Untreated ($n=10$)	30.50 ± 1.13		
Week 16	Negative Control ($n=10$)	5.71 ± 0.26	3.261	0.054
	Positive Control ($n=10$)	27.00 ± 4.50		
	Treatment ($n=10$)	27.80 ± 3.07		
	Untreated ($n=10$)	30.50 ± 1.40		
Week 17	Negative Control ($n=10$)	5.90 ± 0.25	3.180	0.058
	Positive Control ($n=10$)	24.70 ± 6.52		
	Treatment ($n=10$)	24.80 ± 6.18		
	Untreated ($n=10$)	30.00 ± 2.08		
Week 18	Negative Control ($n=10$)	5.87 ± 0.18	5.997	0.007
	Positive Control ($n=10$)	22.20 ± 7.01 *		
	Treatment ($n=10$)	22.70 ± 6.88 *		
	Untreated ($n=10$)	30.20 ± 2.06		

*: Compared with Untreated Group, $P<0.05$;

ganglia (Fig. 6). No obvious shrinkage of the ganglia was observed in the positive control and treatment groups.

The effects of MCC950 on thoracic aorta

The histological examination of the thoracic aorta revealed robust elastic tissue, intact endothelium, and healthy smooth muscle cells in the negative control group (Fig. 7A). In contrast, the positive control group demonstrated moderate preservation of smooth muscle cells with noticeable cytoplasm clearing (Fig. 7B). The MCC950 treatment group exhibited minimal disruption of the endothelial layer and a restoration of smooth muscle integrity (Fig. 7C). However, the untreated group displayed significant endothelial damage, characterized by endothelium breakdown, cytoplasmic clearance in smooth muscle cells, and sub-medial separation (Fig. 7D).

The effects of MCC950 on left ventricle

The Masson trichrome histological examination of the left ventricle revealed the presence of fibrosis, evidenced by collagen deposition (blue staining), in the endocardium, perivascular area, and myocardium (Fig. 8). This staining was markedly prominent in the untreated group. Furthermore, we examined cardiomyocyte morphology by quantifying the cross-sectional area of individual myocytes in H&E-stained sections (Fig. 9). Myocytes in the negative control group retained normal size and an orderly structural appearance. In the positive control, treatment, and untreated diabetic groups, the cells tended to appear smaller, with a gradual reduction in cross-sectional area suggestive of mild cardiomyocyte atrophy. This pattern was visually appreciable across the diabetic groups; however, the group differences did not reach statistical significance.

Discussion

The results obtained from this study underscore the profound impact of streptozotocin administration on fasting blood glucose levels in the experimental rat model of type 1 diabetes mellitus. Hyperglycaemia, a hallmark of T1DM, was successfully induced as early as Week 1 post-STZ injection, persisting throughout the observation period until Week 18. This robust and sustained elevation in blood glucose levels is consistent with clinical observations in diabetic patients and validates the effectiveness of STZ as a pharmacological agent for T1DM induction [21]. Moreover, the observed increase in urine production and polyuria in diabetic rats further supports the establishment of T1DM and underscores the physiological consequences of uncontrolled hyperglycaemia [37].

The concomitant rise in serum NA levels in diabetic rats compared to controls by Week 14 provides additional evidence of DAAS onset. The significant elevation in serum NA levels, a hallmark of sympathetic nervous system dysfunction, is indicative of DAAS progression and underscores the utility of NA as a biomarker for autonomic dysfunction in T1DM [38]. Our results align with these findings, reinforcing the association between hyperglycaemia and autonomic imbalance. Although the increase in serum NA levels at Week 10 did not reach statistical significance, the subsequent rise by Week 14 suggests a progressive deterioration of autonomic function in diabetic rats, highlighting the importance of timely intervention to mitigate DAAS-associated complications [39]. Additionally, similar previous study has reported increased NA levels in diabetic subjects, linking elevated

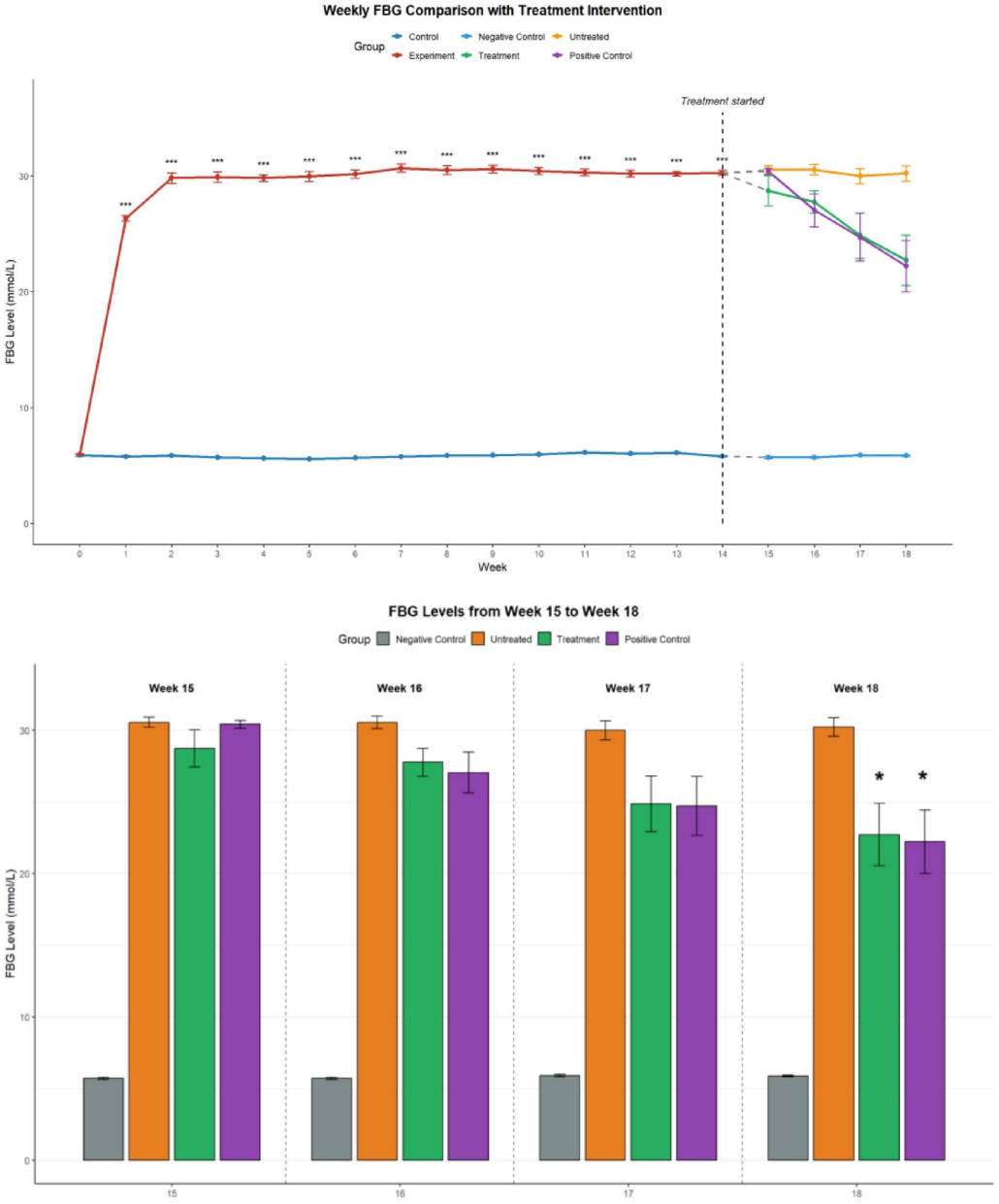

Fig. 5 Trends and intergroup comparisons of FBG levels from Week 15 to Week 18. (*: compared to Untreated Group, $P < 0.05$)

sympathetic activity to DAAS and highlighting the progressive nature of autonomic dysfunction in diabetes [40].

Histological examination of the stellate ganglia revealed significant structural alterations in untreated diabetic rats, characterized by neuronal atrophy and decreased ganglionic size and cell density [20]. These observations are in line with those reported previously who documented similar neuronal damage and atrophy in the autonomic ganglia of diabetic rodents, emphasizing the neurodegenerative impact of chronic hyperglycaemia [41]. In contrast, treatment with MCC950 preserved ganglionic architecture, thereby mitigating neuronal damage and structural alterations within the ganglia. These findings underscore the therapeutic potential of MCC950 in preserving autonomic nerve function and preventing DAAS progression [42].

Similarly, MCC950 treatment attenuated endothelial damage and restored smooth muscle integrity in the thoracic aorta, as evidenced by histological examination. Previous studies has shown that diabetes induces endothelial dysfunction and vascular damage, characterized by impaired endothelial-dependent relaxation and increased oxidative stress [43]. Our results demonstrate that MCC950 can counteract these effects, restoring vascular integrity and function, which is consistent with its

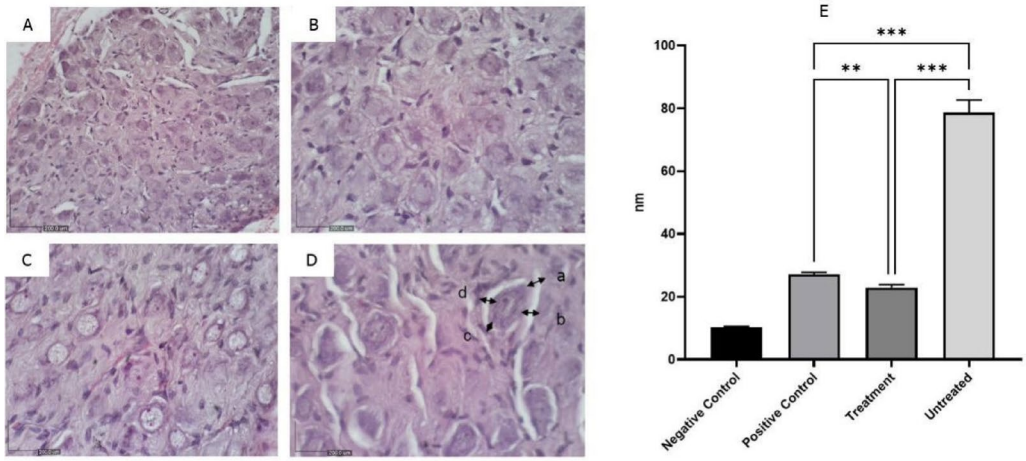

Fig. 6 The architecture of the stellate ganglion was measured using four quadrants of each section (**a**-**d**), and the average measurement was recorded. The negative control group exhibited normal nerve cells with uniform architecture (**A**), while the positive control group (**B**) and treatment group (**C**) showed minimal shrinkage of nerve cells. In contrast, the untreated group exhibited obvious nerve atrophy characterized by a reduction in ganglionic size (**D**). The representation (**A**-**D**) was depicted in a bar graph, with the untreated group (**D**) showing significantly greater shrinkage compared to the positive control and treatment groups (***$p < 0.005$) (X400)

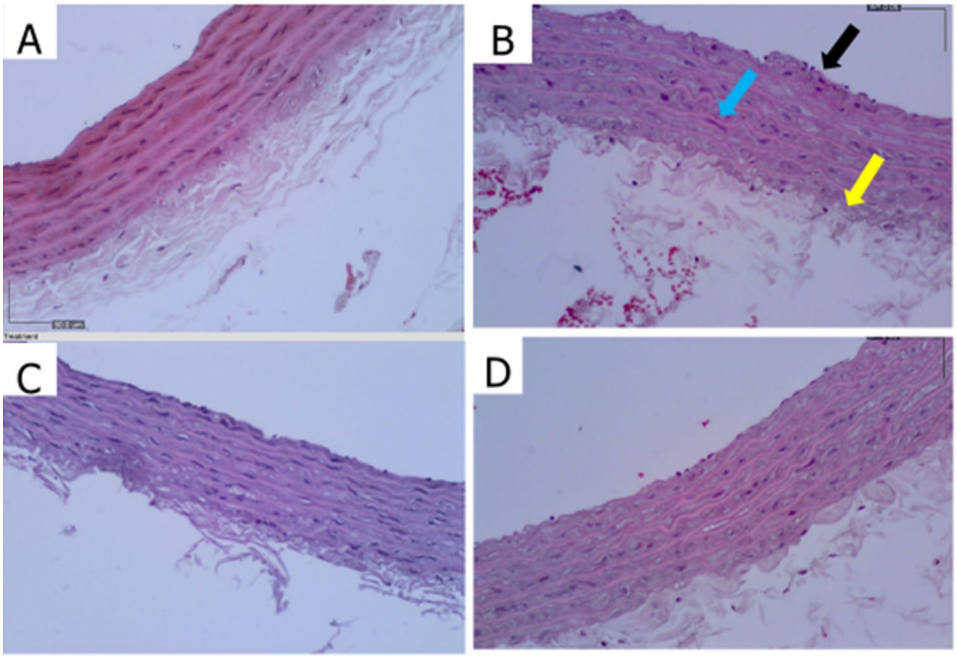

Fig. 7 Negative control (**A**) shows preserved vascular architecture with intact endothelium, well-organized elastic lamellae, and normal smooth muscle cells; Positive control (**B**) demonstrates moderate preservation of smooth muscle cells with cytoplasmic clearing and mild structural alteration; MCC950-treated group (**C**) exhibits minimal disruption of the endothelial layer and improved smooth muscle cell integrity compared with the untreated group;Untreated group (**D**) exhibits intimal endothelium breakdown (red arrow), cytoplasmic clearance of smooth muscle cells (blue arrow), and submedial separation (yellow arrow), indicating significant endothelial damage (×400)

known anti-inflammatory and antioxidant properties [44].

Furthermore, Masson trichrome staining of the left ventricle revealed marked fibrosis in untreated diabetic rats, indicative of adverse cardiac remodelling and myocardial damage. Previous study has highlighted the role of hyperglycaemia-induced oxidative stress and inflammation in promoting myocardial fibrosis in diabetes, leading to compromised cardiac function [45]. Our findings suggest that MCC950 treatment attenuates collagen deposition and preserves myocardial structure, offering a potential therapeutic avenue for mitigating cardiac fibrosis in DAAS [46].

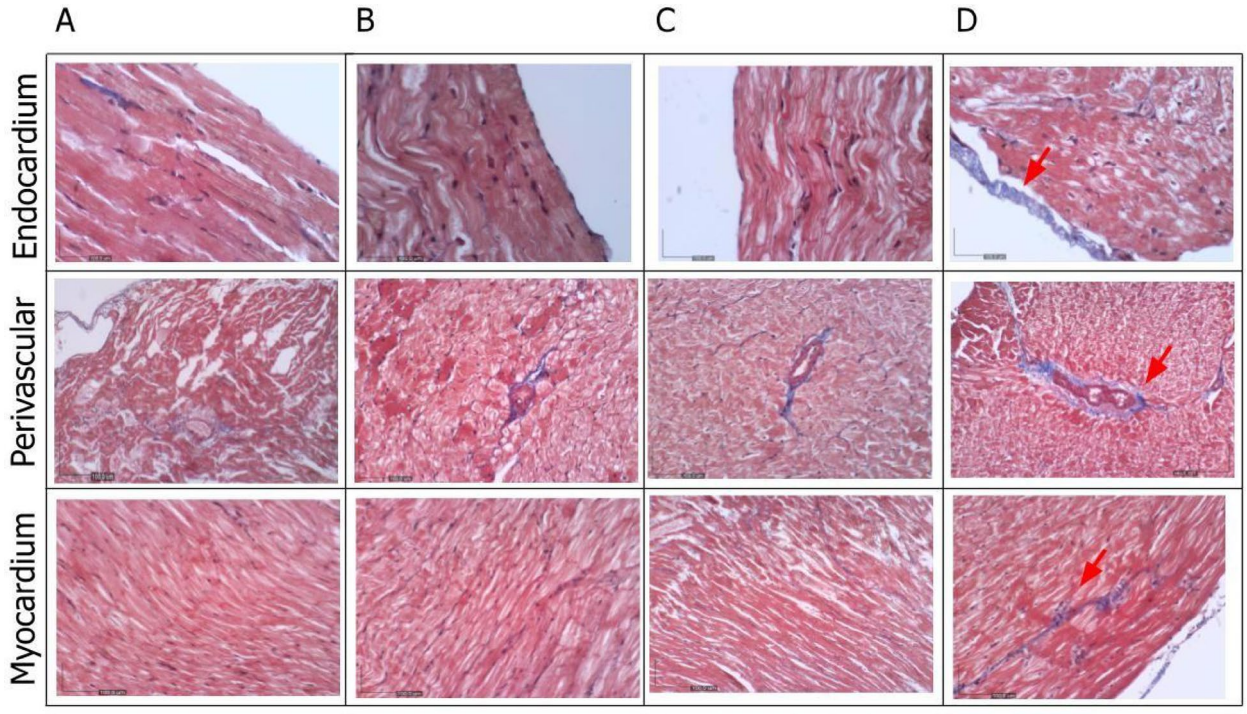

Fig. 8 The qualitative analysis of the Masson trichrome staining revealed the least collagen deposition in the negative control group (**A**), observed in the endocardium, perivascular area, and myocardium. Although there was similar blue staining intensity in both the positive control (**B**) and treatment group (**C**), the intensity of staining (red arrow) was markedly more evident in the untreated group (**D**) (X400)

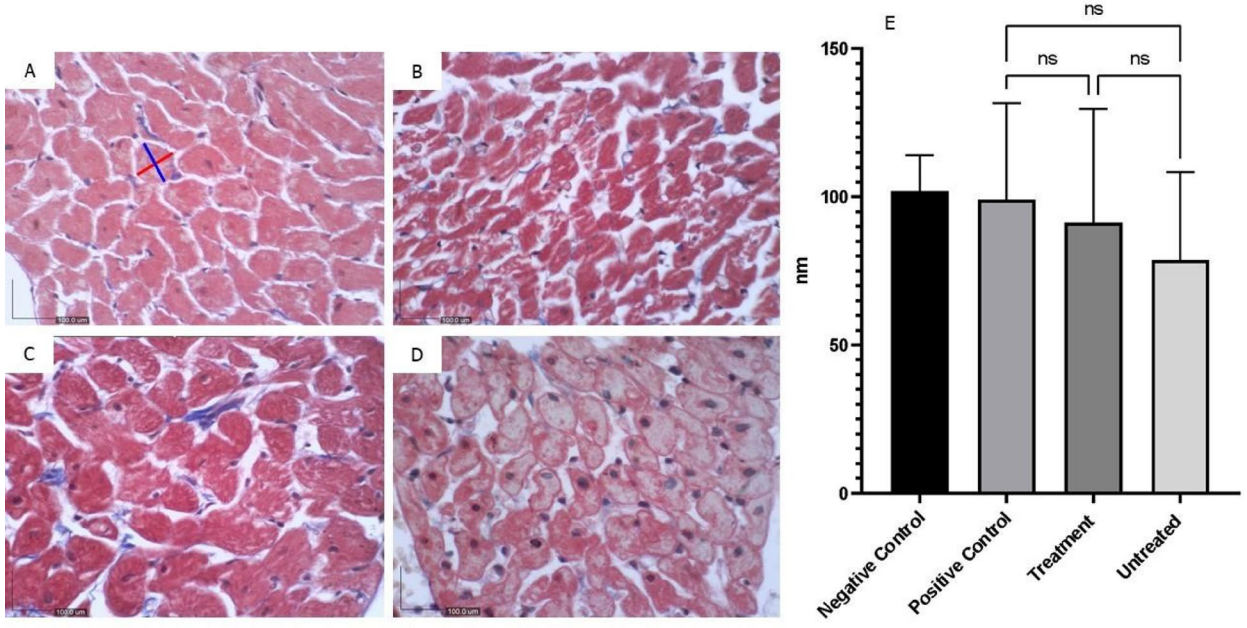

Fig. 9 The cross-sectional area of each cardiomyocyte within a focused microscopy area was measured by averaging the length (measured along the blue line) and width (measured along the red line). The negative control group (**A**) exhibited normal cardiac tissue. Increasing evidence of cardiomyocyte atrophy was observed in the positive control (**B**), treatment (**C**), and untreated group (**D**), respectively. However, these changes were not statistically significant (E) (X400)

Overall, the findings of this study provide valuable insights into the histopathological mechanisms underlying DAAS and highlight the therapeutic potential of MCC950 in attenuating DAAS progression. Our results are consistent with previous research on the detrimental effects of hyperglycaemia on autonomic and cardiovascular health and support the potential of MCC950 as a novel therapeutic agent for DAAS. Further research is warranted to elucidate the molecular mechanisms underlying MCC950's therapeutic effects and validate its efficacy in human trials, ultimately leading to improved clinical outcomes for T1DM patients at risk of DAAS-related complications.

While the study provides valuable insights into the histopathological mechanisms of DAAS and the potential therapeutic effects of MCC950, it primarily relies on preclinical animal models. Translating these findings into clinical applications for human patients may pose challenges due to interspecies variations and the complexity of human physiology compared to animal models.

The study's duration, particularly the treatment period with MCC950, is relatively short. The long-term effects and safety profiles of MCC950 in the context of DAAS management remain unclear. Further investigation with extended observation periods could provide more comprehensive insights into the therapeutic efficacy and potential adverse effects.

Furthermore, the sample size in the experimental groups, particularly for the treatment with MCC950, is relatively small. A larger sample size would enhance the statistical power and generalizability of the findings. Additionally, subgroup analyses based on factors such as age, gender, and disease severity could provide deeper insights into treatment responses.

The study primarily focuses on investigating the therapeutic potential of MCC950 in attenuating DAAS progression. While MCC950 targets inflammation, DAAS is a multifactorial condition influenced by various histopathological mechanisms. Exploring combination therapies or alternative treatment modalities targeting different pathways could offer a more comprehensive approach to DAAS management.

The study relies solely on histological evaluations to assess structural and histopathological changes associated with DAAS and the effects of MCC950 treatment. While histological analyses provide valuable insights, integrating functional assessments such as electrocardiography (ECG), echocardiography, and autonomic function tests could offer a more comprehensive understanding of DAAS progression and treatment responses.

Addressing these limitations in future research endeavours could enhance the validity and clinical applicability of the study findings, ultimately contributing to improved management strategies for DAAS in T1DM patients.

Conclusion

In conclusion, the observed elevation in serum noradrenaline levels by Week 14 provides further evidence of diabetic cardiac autonomic neuropathy onset, highlighting the progressive deterioration of autonomic function in diabetic rats. Histological examination revealed significant structural alterations in the stellate ganglia, thoracic aorta, and left ventricle of untreated diabetic rats, indicative of neuronal damage, vascular dysfunction, and myocardial fibrosis characteristic of DAAS. However, treatment with MCC950 demonstrated promising therapeutic potential in preserving autonomic nerve function, mitigating vascular damage, and attenuating cardiac fibrosis in diabetic rats. These findings underscore the need for further research to elucidate the molecular mechanisms underlying MCC950's therapeutic effects and validate its efficacy in human trials, ultimately offering new avenues for the management of DAAS and improving clinical outcomes for T1DM patients.

Acknowledgements
We extend our gratitude to the dedicated staff members from both departments whose invaluable assistance was instrumental in accomplishing the laboratory work. Special recognition is given to the supporting grant GP/IPM/2022/9739600 and the ethical approval UPM/IACUC/AUP-R015/2023. The article publication charge was funded by the Universiti Kebangsaan Malaysia.

Author contributions
SDS performed the literature review, data curation, data collection, and visualization of results. JC, ZAB, WKH and MAK conducted data collection, statistical analysis, and drafted the initial methods section. XY contributed to the revision and refinement of the manuscript. RA was responsible for conceptualization, funding acquisition, study design, writing the original draft, and final manuscript editing.

Funding
This work was supported by the research grant GP/IPM/2022/9739600.

Data availability
The datasets generated and/or analyzed during the current study are available from the corresponding author on reasonable request.

Declarations

Ethics approval and consent to participate
All experimental procedures were approved by the Institutional Animal Care and Use Committee (IACUC) of Universiti Putra Malaysia (approval number: UPM/IACUC/AUP-R015/2023). The study did not involve human participants; therefore, informed consent was not applicable.

Consent for publication
Not applicable.

Competing interests
The authors declare no competing interests.

Received: 1 July 2025 / Accepted: 18 April 2026
Published online: 11 May 2026

References

1. El Tantawy A, et al. Cardiac autonomic neuropathy linked to left ventricular dysfunction in type 1 diabetic patients. Cardiovasc Endocrinol Metabolism. 2022;11(4):e0272.
2. Sudo SZ, et al. Diabetes-induced cardiac autonomic neuropathy: impact on heart function and prognosis. Biomedicines. 2022;10(12):3258.
3. Svane J, Pedersen-Bjergaard U, Tfelt-Hansen J. Diabetes and the risk of sudden cardiac death. Curr Cardiol Rep. 2020;22:1–10.
4. Bakkar N-MZ, et al. Cardiac autonomic neuropathy: a progressive consequence of chronic low-grade inflammation in type 2 diabetes and related metabolic disorders. Int J Mol Sci. 2020;21(23):9005.
5. Williams S, et al. Cardiac autonomic neuropathy in type 1 and 2 diabetes: epidemiology, pathophysiology, and management. Clin Ther. 2022;44(10):1394–416.
6. Vinik AI, Erbas T, Casellini CM. Diabetic cardiac autonomic neuropathy, inflammation and cardiovascular disease. J Diabetes Investig. 2013;4(1):4–18. https://doi.org/10.1111/jdi.12042 . Epub 2013 Jan 29. PMID: 23550085; PMCID: PMC3580884.
7. Bakkar NZ, Dwaib HS, Fares S, Eid AH, Al-Dhaheri Y, El-Yazbi AF. Cardiac Autonomic Neuropathy: A Progressive Consequence of Chronic Low-Grade Inflammation in Type 2 Diabetes and Related Metabolic Disorders. Int J Mol Sci. 2020;21(23):9005. https://doi.org/10.3390/ijms21239005 . PMID: 33260799; PMCID: PMC7730941.
8. Ang L, Gunaratnam S, Huang Y, Dillon BR, Martin CL, Burant A, Reiss J, Blakely P, Vasbinder A, Zhao L, Mizokami-Stout K, Tang Y, Feldman EL, Doria A, Spino C, Banerjee M, Hayek SS, Pop-Busui R. Inflammatory Markers and Measures of Cardiovascular Autonomic Neuropathy in Type 1 Diabetes. J Am Heart Assoc. 2025;14(1):e036787. Epub 2024 Dec 27. PMID: 39727210; PMCID: PMC12054404.
9. Kaur N, Guan Y, Raja R, Ruiz-Velasco A, Liu W. Mechanisms and Therapeutic Prospects of Diabetic Cardiomyopathy Through the Inflammatory Response. Front Physiol. 2021;12:694864. https://doi.org/10.3389/fphys.2021.694864 . PMID: 34234695; PMCID: PMC8257042.
10. Lanza GA, Pitocco D, Navarese EP, Sestito A, Sgueglia GA, Manto A, Infusino F, Musella T, Ghirlanda G, Crea F. Association between cardiac autonomic dysfunction and inflammation in type 1 diabetic patients: effect of beta-blockade. Eur Heart J. 2007;28(7):814–20. https://doi.org/10.1093/eurheartj/ehm018 . Epub 2007 Mar 19. PMID: 17371783.
11. Sudo SZ, Montagnoli TL, Rocha BS, Santos AD, de Sá MPL, Zapata-Sudo G. Diabetes-Induced Cardiac Autonomic Neuropathy: Impact on Heart Function and Prognosis. Biomedicines. 2022;10(12):3258. https://doi.org/10.3390/biomedicines10123258 . PMID: 36552014; PMCID: PMC9775487.
12. Lei Q, Jiang Z, Shao Y, Liu X, Li X. Stellate ganglion, inflammation, and arrhythmias: a new perspective on neuroimmune regulation. Front Cardiovasc Med. 2024;11:1453127. https://doi.org/10.3389/fcvm.2024.1453127 . PMID: 39328238; PMCID: PMC11424448.
13. Ridwan M, Dimiati H, Syukri M, Lesmana R. Potential molecular mechanism underlying cardiac fibrosis in diabetes mellitus: a narrative review. Egypt Heart J. 2023;75(1):46. https://doi.org/10.1186/s43044-023-00376-z . PMID: 37306727; PMCID: PMC10260731.
14. Serhiyenko V, Serhiyenko A. Diabetic cardiac autonomic neuropathy. In: Dreval AV, Raz I, Grunberger G, eds. The Diabetes Textbook: Clinical Principles, Patient Management and Public Health Issues. Springer. 2023;939–966.
15. Okdahl T, Wegeberg AM, Jensen MM, Quist JS, Brock C. Glycaemic control, low levels of high-density lipoprotein, and high cardiovascular risk are associated with cardiovascular autonomic neuropathy. Diabetol Metab Syndr. 2025;17(1):313. https://doi.org/10.1186/s13098-025-01834-1 . PMID: 40759964; PMCID: PMC12320338.
16. Chindhalore CA, Dakhale GN, Kamble PH, Rathod BD, Kumbhalkar S, Phatak MS. Effect of Ramipril on Cardiac Autonomic Neuropathy in Patients With Type II Diabetes Mellitus. Cureus. 2023;15(3):e36209. https://doi.org/10.7759/cureus.36209 . PMID: 37069873; PMCID: PMC10105262.
17. Razif A, et al. The Evolving Role of Nucleotide-binding Oligomerisation Domain-like Receptor Pyrin Domain 3 Inflammasome Activation in Vascular Endothelial Cells: A Review. Malaysian J Med Sciences: MJMS. 2022;29(2):8.
18. Subramaniam SD, et al. Diabetic Cardiac Autonomic Neuropathy: A Review of NLRP3 Inflammasome Complicity. Mal J Med Health Sci. 2024;20(1):365–8.
19. Wang M, et al. MCC950, a selective NLRP3 inhibitor, attenuates adverse cardiac remodeling following heart failure through improving the cardiometabolic dysfunction in obese mice. Front Cardiovasc Med. 2022;9:727474.
20. Filipović N, et al. Cardiac innervations in diabetes mellitus—Anatomical evidence of neuropathy. Anat Rec. 2023;306(9):2345–65.
21. Ghasemi A, Jeddi S. Streptozotocin as a tool for induction of rat models of diabetes: A practical guide. EXCLI J. 2023;22:274.
22. Dimitropoulos G, Tahrani AA, Stevens MJ. Cardiac autonomic neuropathy in patients with diabetes mellitus. World J diabetes. 2014;5(1):17.
23. Akinlade OM, Owoyele BV, Soladoye OA. Heart rate variability indices, biomarkers, and cardiac nerve density: Independent surrogate markers for diagnosis of diabetic cardiac autonomic neuropathy in type 2 diabetes mellitus animal model. Int J Health Sci. 2020;14(6):24.
24. Al-Assi O et al. Cardiac autonomic neuropathy as a result of mild hypercaloric challenge in absence of signs of diabetes: modulation by antidiabetic drugs. Oxidative Medicine and Cellular Longevity, 2018. 2018.
25. Akinlade OM, Owoyele BV, Soladoye AO. Streptozotocin-induced type 1 and 2 diabetes in rodents: A model for studying diabetic cardiac autonomic neuropathy. Afr Health Sci. 2021;21(2):719–27.
26. Shi L, et al. Beneficial Effects of lncRNA-UC. 360 + shRNA on Diabetic Cardiac Sympathetic Damage via NLRP3 Inflammasome-Induced Pyroptosis in Stellate Ganglion. ACS omega. 2022;7(31):27714–21.
27. Li Z, et al. Elevated glucose metabolism driving pro-inflammatory response in B cells contributes to the progression of type 1 diabetes. Clin Immunol. 2023;255:109729.
28. Oh SS, Narver HL. Mouse and Rat Anesthesia and Analgesia. Curr Protocols. 2024;4(2):e995.
29. Ni B, et al. MCC950, the NLRP3 inhibitor, protects against cartilage degradation in a mouse model of osteoarthritis. Oxidative Med Cell Longev. 2021;2021(1):4139048.
30. Ward R, et al. NLRP3 inflammasome inhibition with MCC950 improves diabetes-mediated cognitive impairment and vasoneuronal remodeling after ischemia. Pharmacol Res. 2019;142:237–50.
31. Yu X-D, et al. Additions to Occultibambusaceae (Pleosporales, Dothideomycetes): Unrevealing Palmicolous Fungi in China. Diversity. 2021;13(11):516.
32. Scherschel K, Bräuninger H, Glufke K, Jungen C, Klöcker N, Meyer C. Location, Dissection, and Analysis of the Murine Stellate Ganglion. J Vis Exp. 2022;(166). https://doi.org/10.3791/62026. PMID: 33427236.
33. Abas R, Othman F, Thent ZC. Protective effect of Momordica charantia fruit extract on hyperglycaemia-induced cardiac fibrosis. Oxidative Medicine and Cellular Longevity, 2014. 2014.
34. Ahmed YM, et al. Partial Synthetic PPARϒ Derivative Ameliorates Aorta Injury in Experimental Diabetic Rats Mediated by Activation of miR-126-5p Pi3k/AKT/PDK 1/mTOR Expression. Pharmaceuticals. 2022;15(10):1175.
35. Ajileye A, Esan E. Fixation and fixatives in histopathology: a review. Bayero J Pure Appl Sci. 2022;15(1):231–43.
36. Li H, Huang J, Liu C, Zhang Z, Song K, Ma K, Dennewitz CW, Wang S. A New Model of Heart Failure Post-Myocardial Infarction in the Rat. J Vis Exp. 2021;(172). https://doi.org/10.3791/62540. PMID: 34180902.
37. Vega-Martín E, et al. Upregulation in Inflammation and Collagen Expression in Perirenal but Not in Mesenteric Adipose Tissue from Diabetic Munich Wistar Frömter Rats. Int J Mol Sci. 2023;24(23):17008.
38. Zhang L-Z, et al. Perioperative changes of serum orphanin in diabetic patients and its relationship with sympathetic nervous system. Neuropeptides. 2024;104:102414.
39. Carmichael J, et al. Advances in screening, early diagnosis and accurate staging of diabetic neuropathy. Front Endocrinol. 2021;12:671257.
40. Voulgari C, et al. Exercise improves cardiac autonomic function in obesity and diabetes. Metabolism. 2013;62(5):609–21.
41. Sima AA, Zhang W. Mechanisms of diabetic neuropathy: axon dysfunction. Handb Clin Neurol. 2014;126:429–42.
42. Amo-Aparicio J, et al. Inhibition of the NLRP3 inflammasome by OLT1177 induces functional protection and myelin preservation after spinal cord injury. Exp Neurol. 2022;347:113889.
43. Subburathinam G. A Study of Endothelial Dysfunction, by Flow Medaiated Vasodialation in Diabetic Patients. Chennai: Madras Medical College; 2020.
44. Romero A, et al. Pharmacological blockade of NLRP3 inflammasome/IL-1β-positive loop mitigates endothelial cell senescence and dysfunction. Aging disease. 2022;13(1):284.
45. Kaur N, et al. Mechanisms and therapeutic prospects of diabetic cardiomyopathy through the inflammatory response. Front Physiol. 2021;12:694864.

46. Bakhshi S, Shamsi S. MCC950 in the treatment of NLRP3-mediated inflammatory diseases: Latest evidence and therapeutic outcomes. Int Immunopharmacol. 2022;106:108595.

Publisher's note